Energy Transport and Nanostructuring of Dielectrics by Femtosecond Laser Pulse Trains

Lan Jiang

Hai-Lung Tsai
e-mail: tsai@umr.edu

Laser-Based Manufacturing Laboratory,
Department of Mechanical and Aerospace Engineering,
University of Missouri-Rolla,
Rolla, MO 65409

This study analyzes single burst ablation of dielectrics by a femtosecond pulse train that consists of one or multiple pulses. It is found that (1) there exist constant-ablation-depth zones with respect to fluence for one or multiple pulses per train and (2) for the same total fluence per train, although the ablation depth decreases in multiple pulses as compared to that of a single pulse, the depth of the constant-ablation-depth zone decreases. In other words, repeatable structures at the desired smaller nanoscales can be achieved in dielectrics by using the femtosecond pulse train technology, even when the laser fluence is subject to fluctuations. The predicted trends are in agreement with published experimental data. [DOI: 10.1115/1.2241979]

Keywords: femtosecond laser, pulse train, quantum mechanics, nanostructure, dielectrics

1 Introduction

An ultrashort (<10 ps) laser pulse can fully ionize almost any solid material and greatly reduce recast, microcracks, and heat-affected zone. Hence, ultrashort lasers are very promising for the micro-/nano-fabrication of all types of materials, especially dielectrics [1–9]. Recent developments of nonlinear optical devices make it possible to obtain almost any arbitrary pulse shapes. Many studies have been reported regarding pulse shaping and its effects on laser-material interactions. For example, by using shaped pulse trains, (1) the ionization process can be controlled [10]; (2) atoms can be selectively ionized [11]; (3) the molecular ground-state rotational dynamics can be manipulated [12]; (4) chemical reactions can be controlled [13]; and (5) the x-ray line emission from plasmas under a femtosecond pulse can be significantly enhanced [14].

These aforementioned abilities of shaped pulse-trains are useful to control and improve micro-/nano-scale processing of dielectrics [3,15,16] and semiconductors [17,18]. Chowdhury et al. [3] conducted pump-probe experiments on femtosecond double-pulse ablation of fused silica through investigating the plasma dynamics at various pulse separation times [3]. Stoian et al. [16] demonstrated an improvement in the quality of femtosecond laser microstructuring of dielectrics by using temporally shaped pulse trains [15]. Stoian et al. [15] further presented the implementation of a self-learning loop on temporal shaping, which again illustrated that under certain excitation conditions, the material response can be guided [16]. The same group showed that this technology is also effective in laser silicon processing and suitable to generate controllable ion beams [17]. Similar work was reported by Choi et al. [18] as well.

Although some explanations were given for possible reasons leading to better ablation quality by pulse train technology, there is no theoretical analysis to directly support the results. As there are many process parameters, such as the pulse profile, pulse separation, number of pulses per train, and fluences, it is very difficult to optimize the process to achieve the best possible ablation quality without a fundamental understanding of the ablation mechanisms.

This study employs the plasma model recently developed by the authors [7–9] to investigate the pulse-train technology, in which quantum theories are employed to calculate the time and space dependent optical and thermal properties, including the electron heat capacity, electron relaxation time, electron conductivity, reflectivity, and absorption coefficient. This paper calculates the ablation of fused silica by a single pulse and pulse-trains consisting of multiple pulses. It is shown that there exist constant-ablation-depth zones with respect to fluence in the femtosecond pulse-train technology by which repeatable nanostructures can be obtained, even when the laser system is subject to fluctuations in fluence.

2 Theory

2.1 Assumptions. Energy transport in the ultrashort laser ablation process can be divided into two stages: (1) the photon energy absorption, mainly through free electron generation and heating, and (2) the redistribution of the absorbed energy to the lattice leading to material removal [4,9]. This stage separation is based on the assumption that free electron generation and heating are completed in such a short time that the lattice temperature remains unchanged within the duration of a femtosecond laser pulse ($\sim$120 fs). The present study is concerned with the first stage of the energy transport, while the lattice temperature remains unchanged in the subpicosecond time regime [7,8].

Building-up of free electrons is necessary to initiate the laser ablation process of dielectrics. It is widely assumed that the ablation starts when the free electron density reaches the critical density [1,6–8,19–22]. For femtosecond lasers, the critical density is selected as the free electron density at which the plasma oscillation frequency is equal to the laser frequency. Once the critical density is created, the originally transparent or semitransparent material becomes opaque, and a large percentage of the absorbed laser energy is deposited in a thin surface layer (tens to thousands of nanometers) within the femtosecond pulse duration [4,20,21]. This leads to the ablation of the thin layer, which starts a few to tens of picoseconds later [4,20–23]. Hence, laser threshold fluence can be considered as the minimal fluence that just creates the critical density [1,6–8,19–22]. Since the free electrons in the thin ablation layer are excited up to tens of electron volts, the Coulomb explosion, electrostatic ablation, or nonequilibrium thermal ablation, instead of melting, dominate after the ionization process [4,5,21]. Thus, under the irradiation of a femtosecond pulse or femtosecond pulse train with subpicosecond-or-shorter pulse

Contributed by the Heat Transfer Division of ASME for publication in the JOURNAL OF HEAT TRANSFER. Manuscript received December 21, 2005; final manuscript received May 2, 2006. Review conducted by Costas Grigoropoulos.

separation time, hydrodynamic (liquid phase) motion of a dielectric is generally negligible. As a result, comparing with long (>10 ps) pulses or pulse trains (including the pulse separation time), melting and recast are greatly reduced and negligible.

This paper investigates a single burst ablation of dielectrics by a femtosecond pulse train with subpicosecond pulse separation, in which a "burst" means the laser irradiation of the whole pulse train may consist of one or multiple pulses. Our calculations are within the single burst irradiation in the subpicosecond time scale before the change of lattice temperature actually happens. In the limit of negligible recast, ablation depth can be considered to be the maximum depth at which the free electron density is equal to the critical density in a given processing window [7,8,19,20]. Similarly, the ablation crater shape corresponds to the ionized region at which the free electron density is greater than or equal to the critical density [7,8,19,20].

2.2 Free Electron Generation: Ionization. The following expression derived from the Fokker-Planck equation is used to calculate the free electron generation [1,6,8,19,20], in which the electron decay term is also considered [1]:

$$\frac{\partial n_e(t,r,z)}{\partial t} = a_i I(t,r,z) n_e(t,r,z) + \delta_N (I(t,r,z))^N - \frac{n_e(t,r,z)}{\tau} \quad (1)$$

where t is the time; r is the distance to the Gaussian beam axis; z is the depth from the surface of the bulk material; τ is the decay time constant; $n_e(t,r,z)$ is the free electron density; a_i is the avalanche ionization constant; $I(t,r,z)$ is the laser intensity inside the bulk material; and δ_N is the cross section of N-photon absorption. Based on experimental measurements of the threshold fluences at the wavelength of 780 nm for fused silica, $a_i = 4 \pm 0.6$ cm^2/J, $\delta_6 = 6 \times 10^{8 \pm 0.9}$ cm^{-3} ps^{-1}(cm^2/TW)^6 [2], and $\tau = 60$ fs [1].

Since the model calculates the electron density distribution within hundreds of femtoseconds, this study ignores electron-lattice energy exchange that is on the order of picoseconds [19]. This assumption was well justified in Refs. [19,20] by experiments and comparison simulations. Also, our related work [24] shows that, for free electron generation in dielectrics, the contribution of electron-phonon interaction is at least two orders of magnitudes smaller than the contribution of ionizations within a femtosecond pulse duration, t_p. Further, the contribution of electron energy diffusion and the electron distribution change because of the Joule heating are, respectively, two and four orders of magnitudes smaller than the contribution of ionization within t_p [24]. Hence, the electron diffusion is also neglected in our model.

2.3 Laser-Plasma Interaction: Optical Properties. The original laser beam before it interacts with the material is assumed to be a Gaussian distribution in time and space. It is assumed that the laser focus point is at the material surface, $z=0$. Considering time and space dependent optical properties, the laser intensities inside the bulk materials are expressed as [7,8]

$$I(t,r,z) = \frac{2F}{\sqrt{\pi/\ln 2}\, t_p}(1 - R(t,r)) \times \exp\left(- \frac{r^2}{r_0^2} - (4 \ln 2)\left(\frac{t}{t_p}\right)^2 - \int_0^z \alpha(t,r,z) dz \right) \quad (2)$$

where F is the laser fluence; t_p is the pulse duration; $R(t,r)$ is the reflectivity; r_0 is the radius of the laser beam that is defined as the distance from the center at which the intensity drops to $1/e^2$ of the maximum intensity; and $\alpha(t,r,z)$ is the absorption coefficient.

The laser intensity distribution inside the material can be determined if the time and space dependent reflectivity and absorption coefficient are obtained. The optical properties of the highly ionized dielectrics under a femtosecond pulse can be well determined by plasma properties [2]. In this study, the Drude model for the plasma in the metals and doped semiconductors is used to determine the optical properties of the ionized dielectrics. The spatial and temporal dependent dielectric function of the plasma is expressed as [25]

$$\boldsymbol{\epsilon}(t,r,z) = 1 + \left(\frac{n_e(t,r,z) e^2}{m_e \boldsymbol{\epsilon}_0} \right) \left(\frac{ - \tau_e^2(t,r,z) + i \tau_e(t,r,z)/\omega}{1 + \omega^2 \tau_e^2(t,r,z)} \right) \quad (3)$$

where e is the electron charge; m_e is the mass of electron; $\boldsymbol{\epsilon}_0$ is the electrical permittivity of free space; $\tau_e(t,r,z)$ is the free electron relaxation time; and ω is the laser frequency. The plasma frequency is defined by [26]

$$\omega_p(n_e) = \sqrt{\frac{n_e(t,r,z) e^2}{m_e \boldsymbol{\epsilon}_0}} \quad (4)$$

At the critical electron density, n_{cr}, the plasma frequency is equal to the laser frequency. Hence,

$$n_{cr} = \frac{4 \pi^2 c^2 m_e \boldsymbol{\epsilon}_0}{\lambda^2 e^2} \quad (5)$$

where c is the scalar speed of light in vacuum and λ is the wavelength of the laser. The complex dielectric function can be split into the real and imaginary components as follows

$$\boldsymbol{\epsilon}(\mathrm{t,r,z}) = \boldsymbol{\epsilon}_1(t,r,z) + i \boldsymbol{\epsilon}_2(t,r,z) = \left(1 - \frac{\omega_p^2(n_e) \tau_e^2(t,r,z)}{1 + \omega^2 \tau_e^2(t,r,z)} \right) + i \left(\frac{\omega_p^2(n_e) \tau_e(t,r,z)}{\omega \left(1 + \omega^2 \tau_e^2(t,r,z) \right)} \right) \quad (6)$$

The relationship between the complex refractive index, $\mathbf{f}$, and the complex dielectric function is given by

$$(\mathbf{c}/\mathbf{v}) = \mathbf{f} = (f_1 + i f_2) = \sqrt{\boldsymbol{\epsilon}} = \sqrt{\boldsymbol{\epsilon}_1 + i \boldsymbol{\epsilon}_2} \quad (7)$$

where $\mathbf{c}$ is the velocity of light in vacuum; $\mathbf{v}$ is the velocity of light in the material; f_1 is the normal refractive index; and f_2 is the extinction coefficient. Thus, the f_1 and f_2 functions are

$$f_1(t,r,z) = \sqrt{\frac{\boldsymbol{\epsilon}_1(t,r,z) + \sqrt{\boldsymbol{\epsilon}_1^2(t,r,z) + \boldsymbol{\epsilon}_2^2(t,r,z)}}{2}}$$
$$f_2(t,r,z) = \sqrt{\frac{ - \boldsymbol{\epsilon}_1(t,r,z) + \sqrt{\boldsymbol{\epsilon}_1^2(t,r,z) + \boldsymbol{\epsilon}_2^2(t,r,z)}}{2}} \quad (8)$$

The reflectivity of the ionized material is determined by the following Fresnel expression at the surface

$$R(t,r) = \frac{(f_1(t,r,0) - 1)^2 + f_2^2(t,r,0)}{(f_1(t,r,0) + 1)^2 + f_2^2(t,r,0)} \quad (9)$$

The absorption coefficient of laser intensity by the plasma via the free electron heating is calculated by

$$\alpha_h(t,r,z) = \frac{2 \omega f_2(t,r,z)}{c} \quad (10)$$

Note that Eq. (10) represents only a part of the laser energy that is absorbed via free electron heating, and there is another part of absorption that is via ionization. The total absorption coefficient, α, accounting for both the free electron heating absorption and the absorption through avalanche ionization and multiphoton ionization is [7]

$$\alpha(t,r,z) = (a_i n_e(t,r,z) + \delta_N (I(t,r,z))^{N-1}) \times (\langle \boldsymbol{\epsilon}(t,r,z) \rangle + U_I) \quad (11)$$

where $\langle \boldsymbol{\epsilon}(t,r,z) \rangle$ is the average kinetic energy of free electrons and U_I is the band gap of materials. For fused silica, $U_I = 9$ eV. Note α in Eq. (11) is used in Eq. (2) in Sec. 2.3 for various pulse absorption mechanisms including free electron heating and generation (ionizations), while α_h in Eq. (10) is used for free electron heating which is explained in Sec. 2.4.

2.4 Free Electron Heating: Electron Relaxation Time. The free electron relaxation time in Eq. (3) is calculated by the following quantum estimation derived from the Boltzmann transport equation [27]

$$\tau_e(t,r,z) = \frac{1}{\nu_{ei}} = \frac{3\sqrt{m_e}(k_B T(t,r,z))^{3/2}}{2\sqrt{2}\pi(Z^*)^2 n_e(t,r,z)e^4 \ln\Lambda} \times (1+\exp(-\mu(n_e,T)/k_B T(t,r,z)))F_{1/2} \quad (12)$$

$$\ln\Lambda = \frac{1}{2}\ln\left(1+\left(\frac{b_{\max}}{b_{\min}}\right)^2\right) \quad (13)$$

where T is the electron temperature, k_B is the Boltzmann's constant, Z^* is the ionization state; μ is chemical potential; $F_{1/2}$ is the Fermi integral. The maximum ($b_{\max}$) and minimum ($b_{\min}$) collision parameters are given by [28]

$$b_{\max} = \frac{(k_B T/m_e)^{1/2}}{\max(\omega,\omega_p)}; \quad b_{\min} = \max\left(\frac{Z^* e^2}{k_B T}, \frac{h}{2\pi(m_e k_B T)^{1/2}}\right) \quad (14)$$

where h is the Planck constant.

However, at the very beginning of laser ablation, the electron kinetic energy is relatively low, and contributions to the free electron relaxation time from electron-phonon collisions could be important. Hence, in this study when the electron kinetic energy is lower than or comparable to the Fermi energy, the contributions of both electron-phonon and electron-ion collisions are considered, and the free electron relaxation time is determined by [28]

$$\tau_e = \frac{1}{\nu_e} = \frac{1}{\nu_{ei}} + \frac{1}{\nu_{ep}} \quad (15)$$

where ν_{ei} is the electron-ion collision frequency and ν_{ep} is the electron-phonon collision frequency determined by

$$\frac{1}{\nu_{ep}} = \left(\frac{M}{m_e}\right)^{1/2}\frac{\hbar}{U_{\rm IP}}\frac{T_D}{T_l}\left(\frac{n_e(t,r,z)}{n_{\rm cr}}\right)^{1/3} \quad (16)$$

where M is the atomic mass unit; $\hbar = h/2\pi$ is the reduced Planck constant; $U_{\rm IP}$ is the ionization potential that is 13.6 eV for fused silica [25]; T_D is the Debye temperature (290 K for fused silica); and T_l is the lattice temperature in K that is assumed to be a constant (300 K, room temperature) during the laser pulse duration. Equation (16) is derived for the plasma with a time-dependent electron density based on Refs. [21,27].

For free electrons modeled as "particle in a box," the chemical potential can be calculated by [26]

$$\mu(n_e,T) = \epsilon_F(n_e) \times \left[1 - \frac{\pi^2}{12}\left(\frac{k_B T(t,r,z)}{\epsilon_F(n_e)}\right)^2 + \frac{\pi^2}{80}\left(\frac{k_B T(t,r,z)}{\epsilon_F(n_e)}\right)^4\right] \quad (17)$$

where the higher order terms are neglected and ϵ_F is the Fermi energy that is determined by

$$\epsilon_F(n_e) = \left(\frac{(hc)^2}{8m_e c^2}\right)\left(\frac{3}{\pi}\right)^{2/3}(n_e(t,r,z))^{2/3} \quad (18)$$

where c is the scalar speed of light in vacuum. And the electron temperatures are determined by

$$c_e(T,n_e)n_e(t,r,z)\frac{\partial T(t,r,z)}{\partial t} = \alpha_h(t,r,z)I(t,r,z) \quad (19)$$

where c_e is the specific heat of free electrons which can be determined by

$$c_e(T_e) = \left(\frac{\partial\langle\epsilon\rangle}{\partial T_e}\right)_V \quad (20)$$

The average kinetic energy, $\langle\epsilon\rangle$, is determined by the Fermi-Dirac distribution

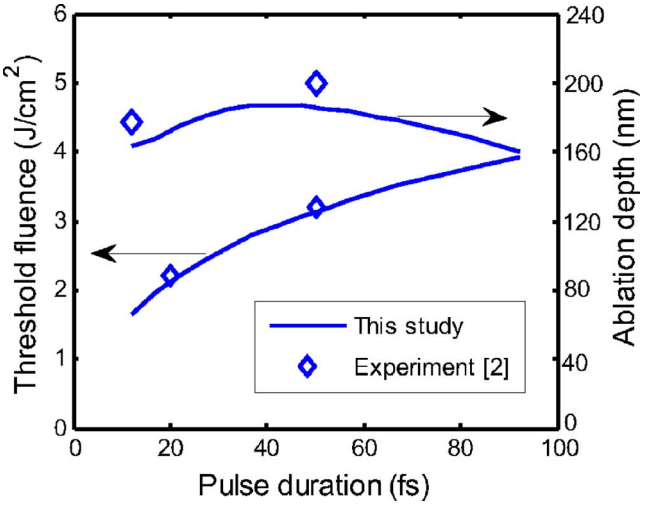

Fig. 1 The theoretical and experimental threshold fluences and ablation depths as a function of pulse duration by a single pulse at the fluence of 5 J/cm^2 and the wavelength of 780 nm

$$\langle\epsilon\rangle = \frac{\sum_k \langle n_k\rangle\epsilon_k}{N_e} = \frac{\int_0^\infty \frac{1}{e^{\beta(T)(\epsilon-\mu(n_e,T))}+1}\rho(\epsilon)\epsilon d\epsilon}{\int_0^\infty \frac{1}{e^{\beta(T)(\epsilon-\mu(n_e,T))}+1}\rho(\epsilon)d\epsilon} \quad (21)$$

where $\beta(T) = 1/k_B T(t,r,z)$ and $\rho(\epsilon)$ is the density of states given by

$$\rho(\epsilon) = \frac{8\sqrt{2}\pi m_e^{3/2}}{h^3}\sqrt{\epsilon} \quad (22)$$

It is assumed that a small volume of material is ablated if its free electron density is equal to or above the critical electron density. The aforementioned equations are solved by an iteration method detailed in Ref. [8].

3 Results and Discussion

3.1 Threshold Fluence, Ablation Depth, and Ablation Shape. Figure 1 shows the threshold fluence and ablation depth as a function of pulse duration for a pulse train consisting of one pulse (a single pulse can also be considered as multipulses with zero pulse separation) at the fluence of 5 J/cm^2 and the wavelength of 780 nm. It is seen that the predictions by the present study are in agreement with the available experimental results at different pulse durations [2]. The validation is not extended into a pulse duration range where the nominal ablation fluence is close to the threshold fluence (and hence the ablation depth is very sensitive to fluence fluctuations). On the other hand, our predictions of the ablation depth and threshold fluence for barium aluminum borosilicate (BBS) in the pulse duration range 40–800 fs are consistent with experimental data. However, due to the page limitation, the results of BBS are not included in this paper.

In our simulations, a train may consist of single or multiple pulses and all have the pulse duration of 50 fs and the wavelength of 780 nm. The pulses within a train have the same fluence. For a train consisting of one pulse, the ablation threshold fluence is found to be 3.3 J/cm^2. For double pulses per train, the ablation thresholds are found to be 1.8, 1.9, and 2.3 J/cm^2 per pulse, i.e., 3.6, 3.8, and 4.6 J/cm^2 per train, at the separation times of 50 fs, 100 fs, and 300 fs, respectively. The ablation shapes are shown in Fig. 2, in which the single pulse at 5 J/cm^2 is also considered as

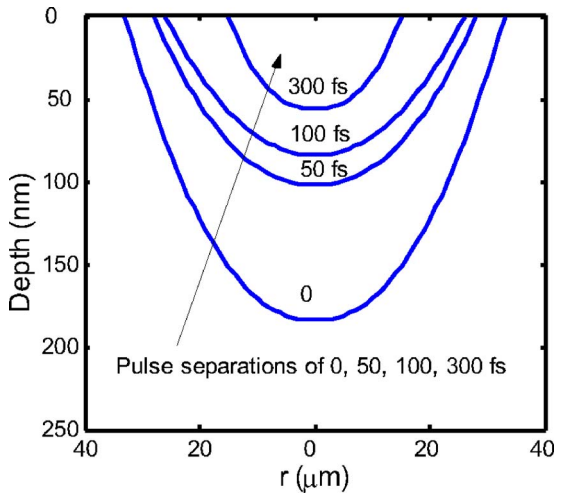

Fig. 2 Ablation crater shapes by pulse trains consisting of double pulses with the total fluence of 5 J/cm^2

a train consisting of double pulses at 2.5 J/cm^2 per pulse with zero pulse separation. At the total fluence of 5 J/cm^2 and the beam spot size of 100 μm, by using the train consisting of double pulses, the ablation depths are 184, 102, 84, and 56 nm, at the pulse separations of 0, 50, 100, and 300 fs, respectively. The ablation depth decreases with the increases of pulse delay, which was also experimentally observed [3]. The corresponding ablation crater diameters for these four cases are 66, 56, 52, and 30 μm, respectively, using the laser beam with a spot size of 100 μm.

It is shown that at the same total fluence, the use of double pulses can obtain smaller structures, which also implies lower throughput as compared to the case of single pulse, which was also observed in experiments [3]. This is because of the lower free electron density as compared to single pulse per train at the same fluence. Specifically, the highest electron density decreases: 3.3×10^{21}, 2.7×10^{21}, 2.6×10^{21}, and 2.2×10^{21} cm^{-3} corresponding to the increases of pulse separation: 0, 50, 100, and 300 fs, respectively. This is due to: (1) the free electrons generated by multiphoton ionization are proportional to I^6 for fused silica at the laser wavelength of 780 nm; (2) the electron decay term in Eq. (1) becomes more significant as the pulse separation time increases; and (3) the surface-generated plasma by the previous pulse(s) interferes with the subsequent pulse(s).

3.2 Transient Localized Free Electron Distribution. The results in Sec. 3.1 demonstrate that it is possible to manipulate transient free electron density distributions inside the dielectrics by shaping pulse train to achieve better ablation quality. The manipulability of energy distribution by the pulse train technology makes it possible to control the transient (femtosecond time scale), localized (nanometer length scale) significantly varying free electron densities of the irradiation area which in turn determines the optical and thermal properties. This is an important reason leading to the advantages of the pulse train technique. As an example, Fig. 3 demonstrates the transient localized properties under a double-pulse burst with the fluence of 2.5 J/cm^2 per pulse and the pulse separation of 100 fs. The calculation starts at the $2t_p$, where t_p is the pulse duration (i.e., 50 fs), before the peak of the first pulse in a train.

The laser intensity distribution at $r=0$ is shown in Fig. 3(a). Under this double-pulse train, the free electron generation is dominated by the first pulse only until 150 fs at which the free electron density reaches about 1.3×10^{20} cm^{-3} as shown in Fig. 3(b). In contrast, the peak free electron density is 2.4×10^{21} cm^{-3}, which is about 18 times greater than the contribution

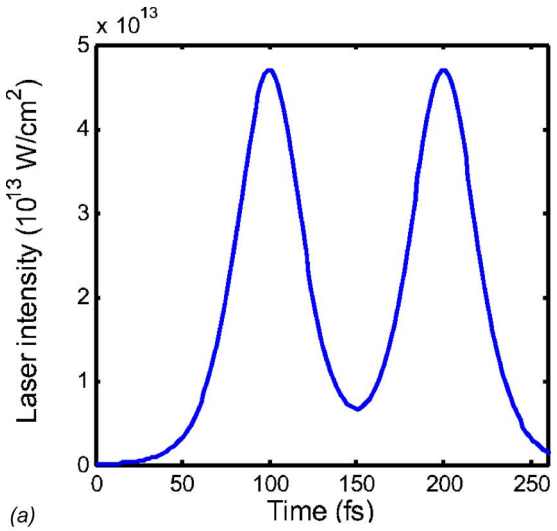

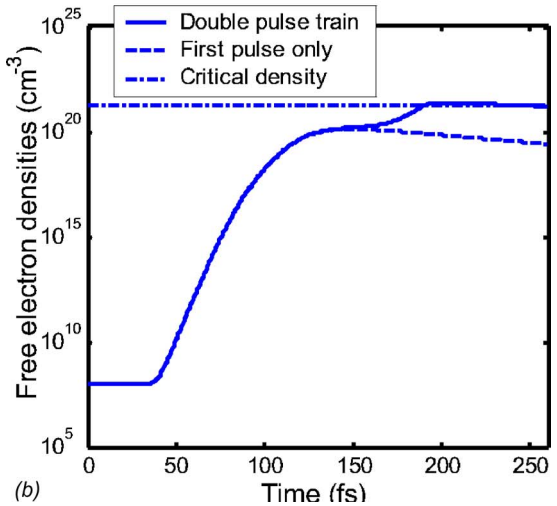

Fig. 3 (a) Laser intensity distribution and (b) electron density at $r=0$, $z=1$ nm for double-pulse train with the total fluence of 5 J/cm^2 and pulse separation of 100 fs

of the first pulse alone. This is mainly due to the enhancement of avalanche ionization process at a higher free electron density [6–8,19,20], i.e., the building-up of free electrons by the first pulse greatly enhances the free electron generation through avalanche ionization during the second pulse. It is possible to achieve the desired electron dynamics (hence optical and thermal properties) by carefully adjusting the pulse train parameters, such as the pulse separation, number of pulses, and pulse fluence distribution, and among which the pulse separation time is convenient to change.

3.3 Pulse Separation Time. The effect of the pulse separation can be visualized through comparisons of the laser intensity distributions as shown in Fig. 4, in which the dashed line represents the original laser energy at $r=0$ before it interacts with the materials and the solid line represents the laser energy transmitted into the material at $r=0$. After the free electron density becomes comparable to the critical density, the original beam profile is strongly shaped by the generated plasma which can be quantified by the transient reflectivity as shown in Fig. 5(a). At $r=0$, the peak reflectivity is 0.95, 0.94, 0.93, and 0.84 for the pulse separations of 0, 50, 100, and 300 fs, respectively, due to lower free

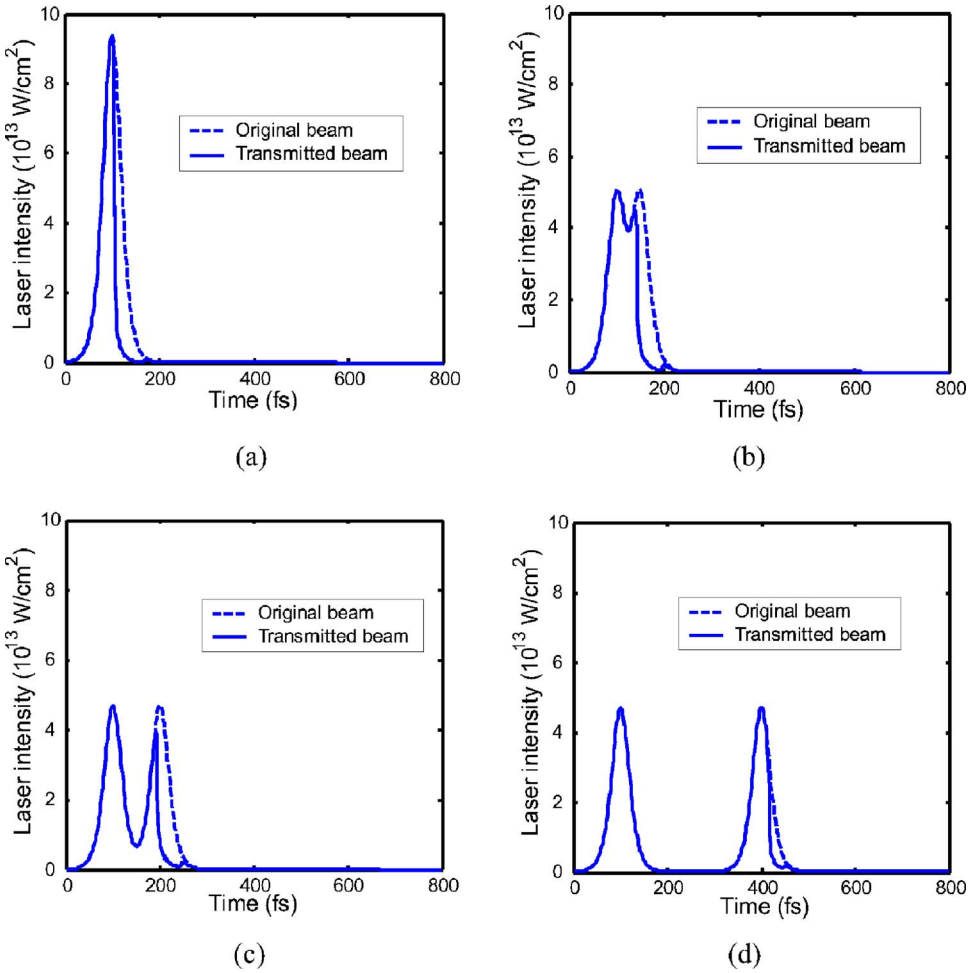

Fig. 4 Center (r=0) laser intensity distributions: (*a*) single pulse per train at 5 J/cm^2 per pulse (also considered as 2 pulses at 2.5 J/cm^2 with 0 pulse separation); (*b*) 2 pulses per train at 2.5 J/cm^2 per pulse (pulse separation is 50 fs); (*c*) 2 pulses per train at 2.5 J/cm^2 per pulse (pulse separation is 100 fs); (*d*) 2 pulses per train at 2.5 J/cm^2 per pulse (pulse separation is 300 fs)

electron density at a longer pulse separation. In contrast, the reflectivity of bulk fused silica is almost zero at the room temperature and the wavelength of 780 nm. Figure 5(*b*) shows the overall reflectivity integrated for the time period during the pulse irradiations. The overall reflectivity significantly decreases as the pulse separation increases. The highest overall reflectivity integrated for the time period during the pulse irradiations is 0.34, 0.29, 0.26, and 0.08 at the separations of 0, 50, 100, and 300 fs, respectively.

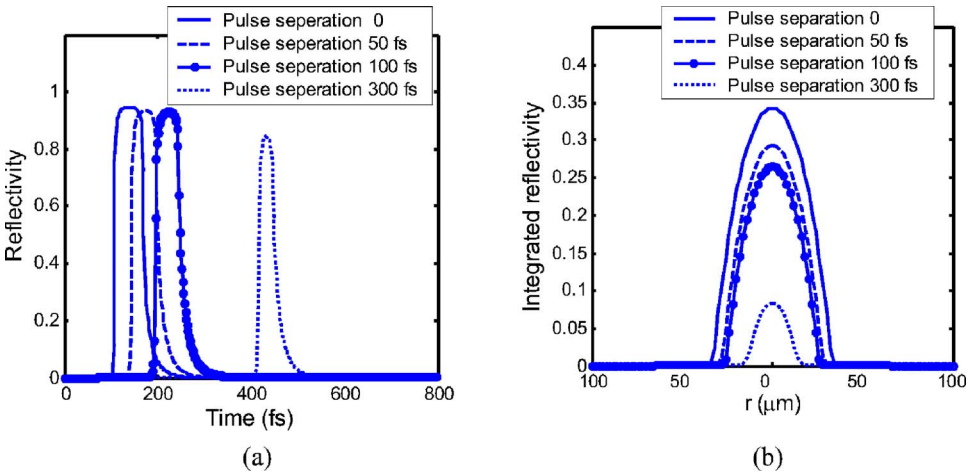

Fig. 5 The reflectivity at r=0 at different pulse separation times: (*a*) transient reflectivity and (*b*) integrated reflectivity

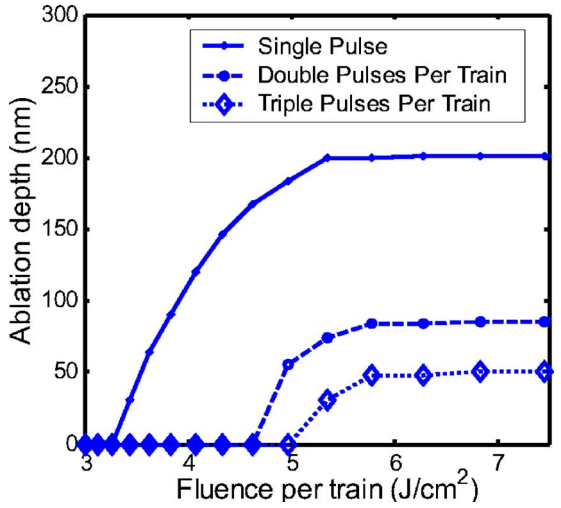

Fig. 6 The ablation depth as a function of total fluence per train; the separation time between pulses for double pulses is 300 fs and for triple pulses is 200 fs

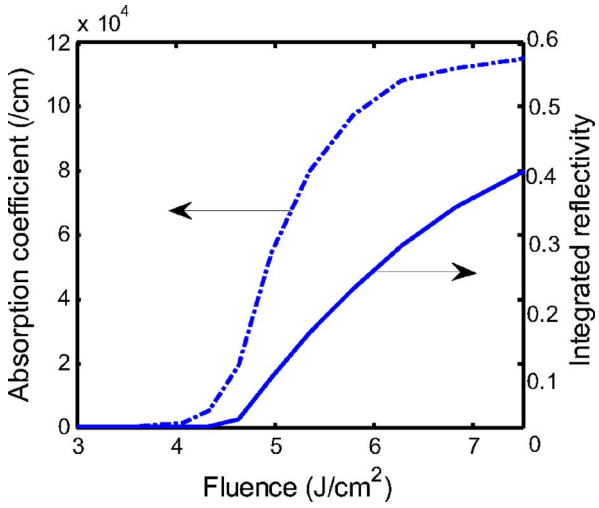

Fig. 7 Surface center integrated reflectivity and absorption coefficient at t=425 fs (the end of the second pulse) under the double-pulse train with separation time of 300 fs

3.4 Fluence. The ablation depth strongly depends on the fluence. For comparison purpose, the fluences in Fig. 6 are in terms of total fluence per train instead of per pulse. As shown in Fig. 6, there are constant-ablation-depth zones with respect to fluences, which are due to the fact that the overall reflectivity and absorption coefficient significantly increase with the increase of fluences [6–8,19,20]. If there exists a constant-ablation-depth zone with respect to fluences, in similar conditions, a flat-bottom crater would be formed under a Gaussian beam, which has been experimentally observed [3,29,30]. Also, a constant-ablation-depth zone with respect to fluences has been directly demonstrated in experiments [31,32]. Note a constant-ablation-depth zone with respect to fluences exists only in a limited fluence range, and the ablation depth may significantly increase if the fluence continues to increase [32,33].

A constant-ablation-depth zone with respect to fluences can be used to improve the repeatability in laser nano-/microfabrications. Laser pulse fluence is subject to fluctuations, which may lead to significant variations in ablation depth especially at fluences slightly above the ablation threshold. Hence, for the case of single pulse per train, it is difficult to control the accuracy for ablation depth below 200 nm as shown in Fig. 6. For example, the ablation depth at 4 ± 0.5 J/cm^2 by a single pulse per train would vary in the range of 47–157 nm. Hence, a slight variation in fluence will result in a large difference in ablation depth. This explains the poor repeatability in the femtosecond ablation of nanostructures using fluences slightly above the ablation threshold [34]. On the other hand, the ablation depth at 6.5 ± 0.5 J/cm^2 is quite stable and is around 200 nm, which is the theoretical limit of repeatable accuracy by the femtosecond single pulse per train for the process window employed in the present study. In contrast, using double pulses per train with the pulse separation time of 300 fs, the ablation depth can be accurately controlled to around 85 nm at 6.5 ± 0.5 J/cm^2, which provides a potential method to achieve repeatable nanostructures. Similarly, using triple pulses per train with the pulse separation time of 200 fs, the ablation depth can be controlled to around 49 nm at 6.5 ± 0.5 J/cm^2. Hence, by using the constant-ablation-depth zones with respect to fluences, repeatable nanostructures at the desired dimension can be obtained, even when the laser system is subject to fluctuations in fluences.

The existence of a constant-ablation-depth zone is caused mainly by the changes of optical properties. As shown in Fig. 7, under the double pulses with separation time of 300 fs, at r=0, and t=425 fs (the end of the second pulse), the absorption coefficients in the surface layer (numerically 1 nm) at the total fluence per train of 4, 5, and 7.5 J/cm^2 are, respectively, 1.6×10^3, 5.6×10^4, and 1.2×10^5 /cm, and the corresponding overall integrated reflectivity are 0.01, 0.08, and 0.4, respectively. Hence, as the total fluence increases, the percentage of the reflected energy increases, and the percentage of the absorbed laser energy deposited in a given thin surface layer also increases. The increase of both the overall reflectivity and the absorption coefficient tend to decrease and attenuate the laser intensity in the material and, as a result, decrease the ablation depth. Hence, roughly speaking, there exists a certain fluence range during which the "negative" effect on ablation depth due to the increases of reflectivity and absorption coefficient "offsets" the increase of the fluence, resulting in a constant-ablation-depth zone. The constant-ablation-depth zone of a pulse train is lower than that of a single pulse per train, as shown in Fig. 7, because for the same total fluence the ablation depth is lowered by a pulse train with multiple pulses.

4 Conclusions

This study employs the validated plasma model with quantum treatments to investigate the pulse-train ablation of dielectrics. The following major conclusions are made from the simulation results:

- The previous pulse has significant effects on the thermal and optical properties for the subsequent pulse within the same train. At the same total fluence, the overall reflectivity significantly decreases as the pulse separation increases.
- The pulse-train technology can obtain smaller structures, although its throughput is relatively low as compared to the case of single pulse at the same total fluence.
- By using constant-ablation-depth zones with respect to fluences in the femtosecond pulse-train technology, repeatable nanostructures at the desired dimension can be obtained, even when the laser system is subject to fluctuations in laser fluences. However, a constant- ablation-depth zone with respect to fluences exists only in a limited fluence range.
- The predicted trends are in agreement with published experimental observations.

Acknowledgment

This work was supported by the Air Force Research Laboratory under Contract No. FA8650-04-C-5704 and the National Science Foundation under Grant No. 0423233.

Nomenclature

a_i = avalanche ionization constant
$b_{\max}$ = maximum collision parameter, Eq. (14)
$b_{\min}$ = minimum collision parameter, Eq. (14)
c = scalar speed of light in vacuum
$\mathbf{c}$ = vector velocity of light in vacuum
c_e = average specific heat per electron
e = electron charge
$\mathbf{f}$ = complex refractive index
f_1 = normal refractive index
f_2 = extinction coefficient
F = laser fluence
h = Planck constant
$\hbar$ = reduced Planck constant
I = laser intensity
k_B = Boltzmann's constant
m_e = nonrelativistic mass of electron
M = atomic mass unit
n_{cr} = critical free electron density
n_e = free electron density
$\langle n_k \rangle$ = average number of electrons in energy state
N = number of photons required in multiphoton ionization
N_e = total number of free electrons
r = distance to the Gaussian beam axis
r_0 = radius of laser beam
R = reflectivity
t = time
t_p = pulse duration
T = free electron temperature
T_D = Debye temperature
T_F = Fermi temperature
T_l = lattice temperature
U_I = band gap energy
U_{IP} = ionization potential
$\mathbf{v}$ = velocity of light in material
z = depth from surface in bulk material
Z^* = charge state of ions

Greek symbols

α = absorption coefficient of free electrons
α_h = absorption coefficient via electron heating
$\rho(\epsilon)$ = the density of states in Eq. (22)
δ_N = cross section of N-photon ionization
ϵ_F = Fermi energy
ϵ_k = energy state
$\langle \epsilon \rangle$ = average electron kinetic energy
$\boldsymbol{\epsilon}$ = complex dielectric function
ϵ_0 = electrical permittivity of free space
ϵ_1 = real component of dielectric function
ϵ_2 = imaginary component of dielectric function
λ = laser wavelength
$\ln \Lambda$ = Coulomb logarithm, Eq. (13)
μ = chemical potential
ν_e = electron collision frequency
ν_{ei} = electron-ion collision frequency
ν_{ep} = electron-phonon collision frequency
ω = laser frequency
ω_p = plasma frequency
τ = electron decay time constant in Eq. (1)
τ_e = free electron relaxation time

References

[1] Li, M., Menon, S., Nibarger, J. P., and Gibson, G. N., 1999, "Ultrafast Electron Dynamics in Femtosecond Optical Breakdown of Dielectrics," Phys. Rev. Lett., **82**, pp. 2394–2397.
[2] Lenzner, M., Krüger, J., Sartania, S., Cheng, Z., Spielmann, C., Mourou, G., Kautek, W., and Krausz, F., 1998, "Femtosecond Optical Breakdown in Dielectrics," Phys. Rev. Lett., **80**, pp. 4076–4079.
[3] Chowdhury, I. H., Xu, X., and Weiner, A. M., 2005, "Ultrafast Double-Pulse Ablation of Fused Silica," Appl. Phys. Lett., **86**, p. 151110.
[4] Jiang, L., and Tsai, H. L., 2003, "Femtosecond Laser Ablation: Challenges and Opportunities," *Proceeding of NSF Workshop on Research Needs in Thermal, Aspects of Material Removal*, Stillwater, OK, pp. 163–177.
[5] Stoian, R., Ashkenasi, D., Rosenfeld, A., and Campbell, E. E. B., 2000, "Coulomb Explosion in Ultrashort Pulsed Laser Ablation of Al_2O_3," Phys. Rev. B, **62**, pp. 13167–13173.
[6] Perry, M. D., Stuart, B. C., Banks, P. S., Feit, M. D., Yanovsky, V., and Rubenchik, A. M., 1999, "Ultrashort-Pulse Laser Machining of Dielectric Materials," J. Appl. Phys., **85**, pp. 6803–6810.
[7] Jiang, L., and Tsai, H. L., 2004, "Prediction of Crater Shape in Femtosecond Laser Ablation of Dielectrics," J. Phys. D, **37**, pp. 1492–1496.
[8] Jiang, L., and Tsai, H. L., 2005, "Energy Transport and Material Removal during Femtosecond Laser Ablation of Wide Bandgap Materials," Int. J. Heat Mass Transfer, **48**, pp. 487–499.
[9] Jiang, L., and Tsai, H. L., 2005, "Improvements on Two-Temperature Models and Its Applications in Ultrashort Laser Damage of Metal Films," ASME J. Heat Transfer, **127**, pp. 1167–1173.
[10] Bartels, R., Backus, S., Zeek, E., Misoguti, L., Vdovin, G., Christov, I. P., Murnane, M. M., and Kapteyn, H. C., 2000, "Shaped-Pulse Optimization of Coherent Emission of High-Harmonic Soft X-rays," Nature (London), **406**, pp. 164–166.
[11] Lindinger, A., Lupulescu, C., Plewicki, M., Vetter, F., Merli, A., Weber, M. S., and Wöste, L., 2004, "Isotope Selective Ionization by Optimal Control Using Shaped Femtosecond Laser Pulses," Phys. Rev. Lett., **93**, p. 033001.
[12] Renard, M., Hertz, E., Lavorel, B., and Faucher, O., 2004, "Controlling Ground-State Rotational Dynamics of Molecules by Shaped Femtosecond Laser Pulses," Phys. Rev. A, **69**, p. 043401.
[13] Assion, A., Baumert, T., Bergt, M., Brixner, T., Kiefer, B., Seyfried, V. V., Strehle, M., and Gerber, G., 1998, "Control of Chemical Reactions by Feedback-Optimized Phase-Shaped Femtosecond Laser Pulses," Science, **282**, pp. 919–922.
[14] Andreev, A. A., Limpouch, J., Iskakov, A. B., and Nakano, H., 2002, "Enhancement of X- ray Line Emission from Plasmas Produced by Short High-Intensity Laser Double Pulses," Phys. Rev. E, **65**, p. 026403.
[15] Stoian, R., Mermillod-Blondin, A., Winkler, S., Rosenfeld, A., Hertel, I. V., Spyridaki, M., Koudoumas, E., Fotakis, C., Burakov, I. M., and Bulgakova, N. M., 2004, "Temporal Pulse Manipulation and Adaptive Optimization in Ultrafast Laser Processing of Materials," Proc. SPIE, **5662**, pp. 593–602.
[16] Stoian, R., Boyle, M., Thoss, A., Rosenfeld, A., Korn, G., Hertel, I. V., and Campbell, E. E. B., 2002, "Laser Ablation of Dielectrics With Temporally Shaped Femtosecond Pulses," Appl. Phys. Lett., **80**, pp. 353–355.
[17] Spyridaki, M., Koudoumas, E., Tzanetakis, P., Fotakis, C., Stoian, R., Rosenfeld, A., and Hertel, I. V., 2003, "Temporal Pulse Manipulation and Ion Generation in Ultrafast Laser Ablation of Silicon," Appl. Phys. Lett., **83**, pp. 1474–1476.
[18] Choi, T. Y., Hwang, D. J., and Grigoropoulos, C. P., 2002, "Femtosecond Laser Induced Ablation of Crystalline Silicon upon Double Beam Irradiation," Appl. Surf. Sci., **197-198**, pp. 720–725.
[19] Stuart, B. C., Feit, M. D., Herman, S., Rubenchik, A. M., Shore, B. W., and Perry, M. D., 1996, "Nanosecond-to-Femtosecond Laser-Induced Breakdown in Dielectrics," Phys. Rev. B, **53**, pp. 1749–1761.
[20] Stuart, B. C., Feit, M. D., Rubenchik, A. M., Shore, B. W., and Perry, M. D., 1995, "Laser-Induced Damage in Dielectrics With Nanosecond to Subpicosecond Pulses," Phys. Rev. Lett., **74**, pp. 2248–2251.
[21] Gamaly, E. G., Rode, A. V., Luther-Davies, B., and Tikhonchuk, V. T., 2002, "Ablation of Solids by Femtosecond Lasers: Ablation Mechanism and Ablation Thresholds for Metals and Dielectrics," Phys. Plasmas, **9**, pp. 949–957.
[22] Du, D., Liu, X., Korn, G., Squier, J., and Mourou, G., 1994, "Laser-Induced Breakdown by Impact Ionization in SiO_2 With Pulse Widths From 7 ns to 150 fs," Appl. Phys. Lett., **64**, pp. 3071–3074.
[23] Rethfeld, B., Kaiser, A., Vicanek, M., and Simon, G., 2002, "Ultrafast Dynamics of Nonequilibrium Electrons in Metals Under Femtosecond Laser Irradiation," Phys. Rev. B, **65**, p. 214303.
[24] Jiang, L., and Tsai, H. L., 2006, "Plasma Modeling for Femtosecond Laser Ablation of Dielectrics," J. Appl. Phys., **100**(2), p. 023116.
[25] Fox, M., 2001, *Optical Properties of Solids*, Oxford University Press, Oxford.
[26] Ashcroft, N. W., and Mermin, N. D., 1976, *Solid State Physics*, Holt, Rinehart.
[27] Lee, Y. T., and More, R. M., 1984, "An Electron Conductivity Model for Dense Plasma," Phys. Fluids, **27**(5), pp. 1273–1286.
[28] Eidmann, K., Meyer-ter-Vehn, J., Schlegel, T., and Hüller, S., 2000, "Hydrodynamic Simulation of Subpicosecond Laser Interaction With Solid-Density Matter," Phys. Rev. E, **62**, pp. 1202–1214.

[29] Wu, Z., Jiang, H., Zhang, Z., Sun, Q., Yang, H., and Gong, Q., 2002, "Morphological Investigation at the Front and Rear Surfaces of Fused Silica Processed With Femtosecond Laser Pulses in Air," Opt. Express, **10**, pp. 1244–1249.
[30] Bonse, J., Munz, M., and Sturm, H., 2004, "Scanning Force Microscopic Investigations of the Femtosecond Laser Pulse Irradiation of Indium Phosphide in Air," IEEE Trans. Nanotechnol., **3**, pp. 358–367.
[31] Nakamura, S., Hoshino, M., and Ito, Y., 2001, "Monitoring of CW YAG Laser Welding Using Optical and Acoustic Signals," *Proceedings of ICALEO*, Jacksonville, FL.
[32] Lapczyna, M., Chen, K. P., Herman, P. R., Tan, H. W., and Marjoribanks, R. S., 1999, "Ultra High Repetition Rate (133 MHz) Laser Ablation of Aluminum With 1:2-ps Pulses," Appl. Phys. A: Mater. Sci. Process., **69**, pp. S883–S886.
[33] Herman, P. R., Oettl, A., Chen, K. P., and Marjoribanks, R. S., 1999, "Laser Micromachining of 'Transparent' Fused Silica With 1-ps Pulses and Pulse Trains," Proc. SPIE, **3616**, pp. 148–155.
[34] Chichkov, B. N., Ostendorf, A., Korte, F., and Nolte, S., 2001, "Femtosecond Laser Ablation and Nanostructuring," *Proceedings of ICALEO*, Jacksonville, FL.